Using rocking frequencies of bridge piers for scour monitoring

Nissrine Boujia, Franziska Schmidt, Christophe Chevalier, Dominique Siegert, Damien Pham van Bang

Using rocking frequencies of bridge piers for scour monitoring

Nissrine Boujia[1], Franziska Schmidt [1,*], Christophe Chevalier [2], Dominique Siegert [3] and Damien Pham Van Bang [4]

1 MAST-EMGCU, Université Gustave Eiffel, IFSTTAR, Cité Descartes - Bâtiment Bienvenüe, 14-20 Boulevard Newton, F-77447 Champs sur Marne - Marne-la-Vallée cedex 2, France ;

2 GERS-SRO, Université Gustave Eiffel, IFSTTAR, Cité Descartes - Bâtiment Bienvenüe, 14-20 Boulevard Newton, F-77447 Champs sur Marne - Marne-la-Vallée cedex 2, France ;

3 COSYS-LISIS, Université Gustave Eiffel, IFSTTAR, Cité Descartes - Bâtiment Bienvenüe, 14-20 Boulevard Newton, F-77447 Champs sur Marne - Marne-la-Vallée cedex 2, France ;

4 INRS, Centre Eau Terre Environnement, Québec, QC G1K 9A9, Canada; damien.pham_van_bang@ete.inrs.ca

* Correspondence: franziska.schmidt@univ-eiffel.fr

In this study, scour-based vibrations of bridge piers are investigated using a bridge model in a water flume: first, the eigenmode corresponding to the measured frequencies of pier-like structures is identified. Secondly, the effect of the pier-deck interaction is studied. Finally, a theoretical model is proposed to characterize the pier vibration, and identify its input parameters.

To this end, experimental campaigns were conducted and a laboratory scale model pier was tested in two configurations: single piers and two piers in bridge configuration. The experimental results enable the identification of the modal shape and indicate that the deck decreases significantly the pier's frequency. Parallely, a theoretical model was proposed to model the pier, where the soil was modeled with both lateral springs along the pier and a rotational spring at the base.

These springs stiffness were then identified using a 3D-finite element model. These results, obtained with the theoretical and numerical models, are in good agreement with the experimental results with the bridge pier in the two tested configurations. Moreover the obtained theoretical, numerical and experimental results were compared to experimental data found in the literature, for further validation.

Keywords— Scour, soil-structure interaction, pier-deck interaction, modal shapes, rigid modes, monitoring.

Abbreviations:

b	Pier diameter [m]
D	Embedded length [m]
D_{50}	Average grains diameter [m]
E_s	Soil's Young modulus [MN/m ^{2}]
E_p	Pier's Young modulus [MN/m ^{2}]
f	Pier frequency [Hz]

h_0	Water height [m]
H	Exposed length [m]
J_G	Moment of inertia [Kg.m ^{2}]
k_s	Horizontal stiffness of the soil [MN/m ^{2}]
K	Horizontal spring stiffness [MN/m]
K_r	Rotational spring stiffness [MN.m/rad]
L	Pier total length [m]
L_1	Distance between the center inertia and the pier base [m]
m	Pier total weight [Kg]
M	Deck total weight [Kg]
α	Slenderness ratio [-]
ν_s	Soil Poisson ratio [-]
ρ	Soil bulk density [Kg/m ^{2}]
ω	Pulse $2\pi f$
x	Gravity center lateral displacement [m]
θ	Gravity center rotation [rad]

1 Background

Scour is the erosive action of water carrying away sediment of the riverbed. Around bridge supports, scour holes are created, undermining the foundations and decreasing the bearing capacity of the soil. As a consequence, scour is the main cause of bridge failures in many countries [1, 2]. Thus, in order to address this risk, various monitoring techniques have been developed and tested on field. In early days, geophysical tools such as radar and sonar [3, 4, 5, 6] were most commonly used. Various monitoring techniques use magnetic field properties and includes sensors such as the magnetic sliding collar [7] and smart rocks [8]. The main limitations of these monitoring techniques are their sensitivity to suspended sediments and their vulnerability in harsh environment which is major hurdle to continuous scour monitoring.

Recently, the use of dynamic behaviour-based techniques to measure scour depth has been confirmed as a promising alternative to the previous techniques. Two approaches can be identified, namely an indirect and direct approach. The indirect approach consists in placing rod-sensors around the bridge piles and monitor their frequency [9, 10]. As scour increases, the first frequency of the sensor decreases [11].

The direct approach consists in monitoring the frequency of the bridge structure itself. [12] performed impact tests on railway bridges to assess their foundation conditions. The results indicate that the more the piers are scoured, the lower their frequencies, with definition of a limit numerical value of the frequency making it possible to discriminate damaged piers from those in good health. [13] studied the effect of scour on the modal parameters of a five spans bridge in Italy. This study showed that the frequencies and modal shapes of the spans are highly affected by scouras also reported by various other authors [14, 15]. [16] studied the effect of scour on a single pile (slenderness $\alpha > 10$) and developed a 2D-model based on the Winkler theory [17] for Soil-Structure Interaction to estimate the variation of the pile frequency with scour depth. Thus, the soil-pile interaction was modeled by a beam exposed to horizontal independent linear springs

which were progressively removed to take into account scour. The proposed model was able to give a good prediction of the evolution of the single pile frequency with scour. However, it is difficult to extend this model to the case of a bridge pier. In fact, on the one hand bridge piers are rarely slender as this given pile [16]. One the other hand, the pier stiffness with respect to soil stiffness is usually very high. A recent experimental study of [18] studied the effect of scour on the vibration of a laboratory-scale concrete column (slenderness $\alpha = 2$). The results show that, indeed, the first frequency of the column decreases with scour and can be used for scour monitoring. However, open points in this study can be identified : First, the modal shape of the pier corresponding to the identified frequency was not determined. Then, even though the characteristics of the tested single pier were closer to those of a real bridge pier, the pier-deck interaction was not taken into account. Finally, no physical model was proposed in order to estimate the frequency of this kind of structures for various scour depths.

The present paper addresses some open issues in this topic: First, we determine the physical meaning of the measured frequency : When monitoring the vibration frequency of slender and flexible structures, such as piles, it is easy to visualize the modal shape corresponding to their bending mode. For rigid structures, such as piers, it is more complex to understand exactly the kinematics of the modal shapes. Then, we will study the effect of the presence of the deck on the pier frequency and its sensitivity to scour. Finally, we will try to establish whether or not it is adequate to model the soil-pier by horizontal springs only, considering the aspect ratio between the lateral faces and the base of a cylindrical pier.

The paper starts with a description of the experimental campaigns that have been undertaken in a water flume. The experimental results are then presented in Section 2. In Section 3, a theoretical formulation for the soil-pier interaction is proposed and a sensitivity study of the dynamic response of the piers to the slenderness ratio and soil stiffness is performed. In Section 4, a comparison between the numerical and experimental results is presented. Finally, the main achievements of this work are summarized.

2 Experimental campaigns

The dynamic behaviour of reduced-scale bridge piers is analyzed in a water flume, with and without water, before studying a reduced-scale, one-span bridge.

2.1 Single bridge pier tests

A laboratory scale model bridge pier is made in order to assess the effect of scour on its frequency f. The concrete pier is cylindrical and has a total length $L = 55$ cm and a diameter $b = 11$ cm, which are the reduced dimensions of the piers of a prestressed concrete bridge near Orléans [19].

2.1.1 Dry sand tests on a single pile

The experimental set-up is presented in Figure 1 : A tank of dimensions $1m \times 1m \times 1m$ is progressively filled with dry sand of Seine until it reaches a height of 0.7 m. The pier is then placed in the middle of the sand volume to avoid edge effects, with an embedded length D. A tri-axial, high-sensitivity accelerometer is placed at the top of the pier and records its response with a sampling frequency of 25.6kHz. It is connected to a data-acquisition card from National Instruments, controlled with LabVIEW. A symmetric scour hole is then created by progressively

extracting a 5 cm-thick soil layer, so that the embedded length of the pier varies from 25 to 5 cm. For each embedded length D, an impact is applied with a calibrated impact hammer and the response of the pier in the horizontal direction x is recorded by the accelerometer.

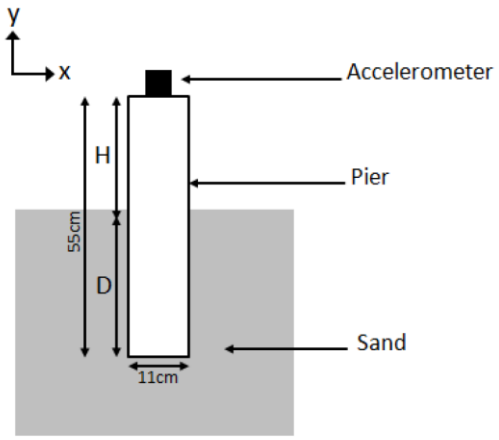

Figure 1: Experimental setup of single pier, dray sand tests.

2.1.2 Single pier, water flume tests

The next series of experiment are conducted in a water flume : The flume is progressively filled with Hostun sand ($D_{50} = 0.6$ mm) until it reaches a final height of 25 cm. The pier is then placed with an initial embedded length $D = 20$ cm (Figure 2). The flow velocity is progressively increased to generate a scour hole. The acceleration of the pier in the flow direction x is recorded with two accelerometers (Figure 2), which will be used to identify the modal shapes corresponding to the measured frequencies of the pier.

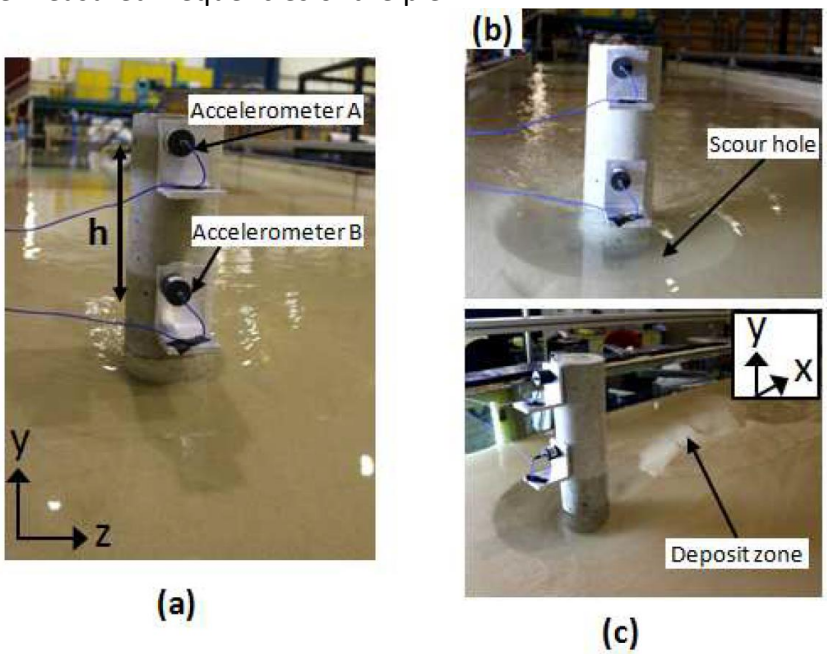

Figure 2: Experimental setup of single piers, water flume tests : (a) the initial configuration without scour (h the distance between the two accelerometers) (b) front view and (c) side view of the scoured configuration.

Two different testing protocols are applied : The first protocol consists in applying a hammer impact, as in the laboratory tests, at regular intervals of scour depth. For the second

experimental protocol, the flow induced vibrations of the pier are recorded all along the scouring process.

2.2 Reduced-scale bridge model tests

For the final series of tests, a bridge configuration (Figure 3) is tested to assess the effect of the pier-deck interaction on the first frequency of the pier. Two bridge piers distant of 140 cm are place in the flume with an initial embedded length $D = 20$ cm. Rubber bearings are then placed on the top of each pier and the model bridge deck is placed over the two rubber bearings. The length of the deck is 160 cm and its total weight is $M = 26$ Kg. A hammer impact is applied at the middle of the deck at regular intervals of scour depth and the piers accelerations, in the flow direction x, are recorded with two accelerometers.

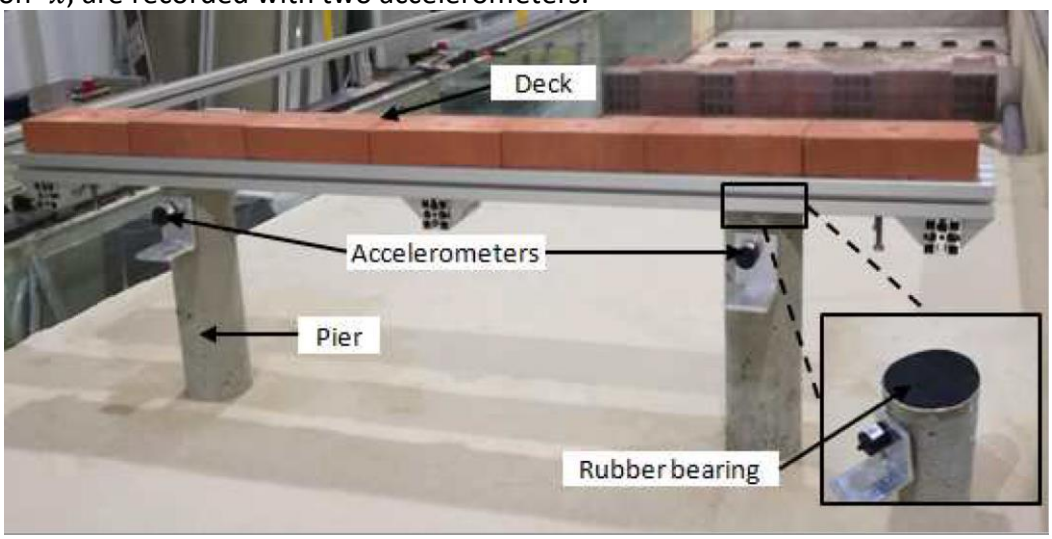

Figure 3: Experimental setup of the bridge configuration tests.

3 Experimental results

3.1 Effect of scour on the first frequency of the pier

The accelerations of the pier, measured by the accelerometers in all tested configurations presented in Section 2, contain a large number of high frequencies. Therefore, the signal is first filtered using a 4th order low-pass Butterworth filter with a cut-off frequency of 100 Hz, which makes it possible to capture the structural response of the pier . Then, the first frequency f of the pier is calculated using a Fast Fourier Transform (FFT).

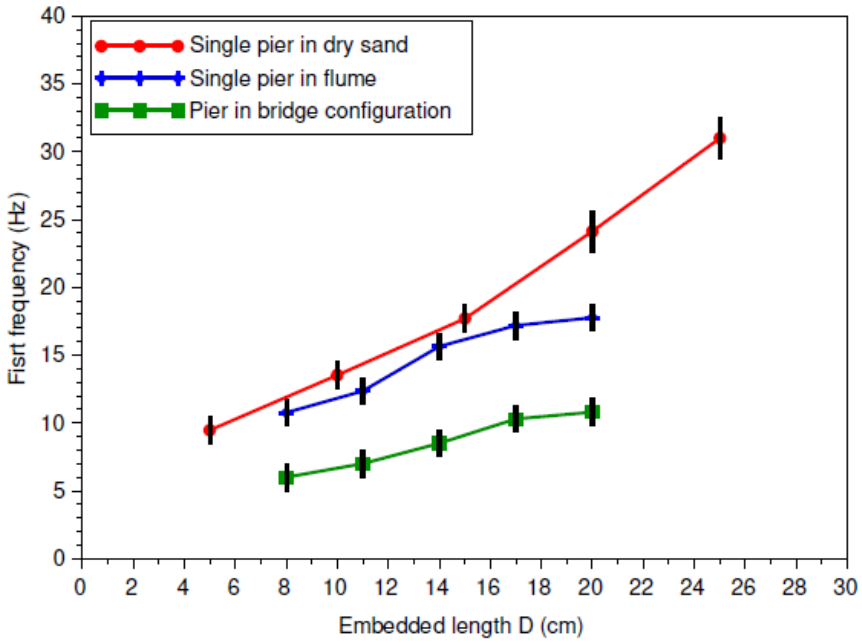

Figure 4: Variation of the frequency with the embedded length D, in dry sand and flume tests with and without the deck.

The variation of the first frequency f of the pier with the maximum scour depth in dry sand, in flume without the deck and in the bridge configuration are as expected (Figure 4) : as scour depth increases, meaning as the embedded length D decreases, the first frequency of the pier decreases. However, the results also show that the frequency of the pier in the flume, with and without the deck, remains steady for the first scoured centimeters. One possible reason for this insensitivity to scour is that the first layer of the soil is very loose : when conducting the test, the flow is first kept steady until the water reaches the required level of $h_0 = 7.5$cm. During this initial phase and since the water level is very low at the beginning, the pier is scoured, up to 5cm in our configuration. Once the required water level is reached, sand is moved back to fill the hole and the impact tests are performed. However, since no compaction of the added soil is possible, this layer of the soil remains loose and may not insure much constraint to the pier.

Regarding the effect of the deck on the pier's frequency, the experimental results (Figure 4) show a significant decrease in the frequencies : the frequencies of the pier in the bridge configuration are less by about 35% compared to the frequencies of the single pier.

The sensitivity of the pier's frequency to scour in the two tested configurations is compared : to achieve that, the variation ratio of the frequency $|\Delta f|/f_0$ ($\Delta f = f - f_0$ where f is the measured frequency for a given scour depth and f_0 is the frequency of the pier without scour) is calculated for each scour depth. The results (Table 1) indicate that the sensitivity of the pier to scour does not change significantly when taking into account the pile-deck interaction.

Scour depth (cm)	$\lvert\Delta f\rvert/f_0$ (%)	
	Single pier	Pier with the deck
0	0	0
3	0	4
6	13	21
9	31	35
12	40	44

Table 1: Frequency variation with scour depth of the single pier and the pier in a bridge configuration.

3.2 Identification of the modal shape of the pier

The tested pier has a slenderness ratio $\alpha = 5$ and its stiffness with respect to the soil stiffness is $E_p/E_s > 10^3$, where E_p is the Young modulus of the pier and E_s the Young modulus of the soil. Under impact tests, the pier vibrates following a rigid-body motion given its slenderness and stiffness. Thus, placing two accelerometers on the pier is sufficient to determine the mode shapes corresponding to the measured first frequency.

First, the first frequency of the pier is calculated using a Fast Fourier Transform (FFT). The signal is then filtered using a low pass filter (Figure 5 (a), (b), (c)) to make sure that the measured accelerations correspond to the first frequency only and therefore, the first modal shape. The modal shapes are normalized to the maximum displacement. The normalized modal shapes for different embedded lengths D are plotted in Figure 5 (d). The results show that the governing motion of the pier is a coupled swaying-rocking mode with a center of rotation embedded in the soil. However, the variation of the modal shape with scour is insignificant.

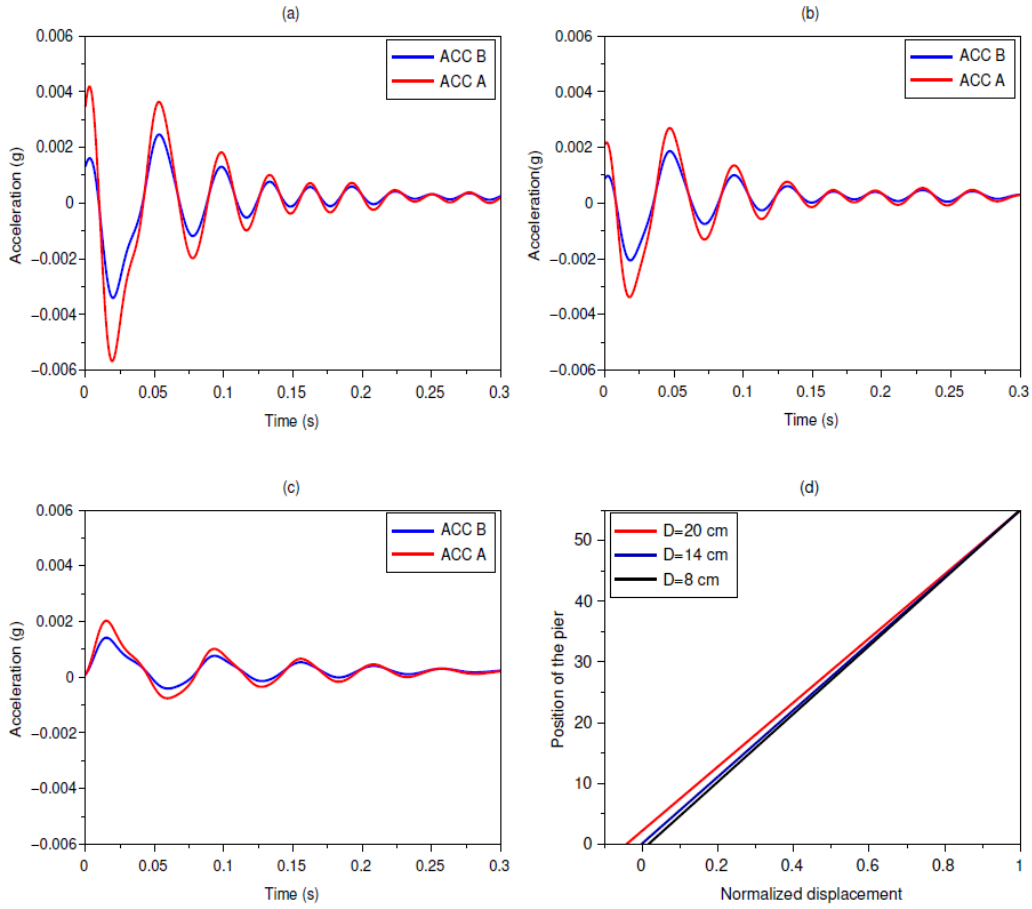

Figure 5: The filtered accelerations recorded with the accelerometer A and B (labels « ACC A » and « ACC B ») for the embedded lengths (a) D=20cm, (b) D=14cm and (c) D=8cm and (d) the corresponding modal shapes.

4 Proposed theoretical model

4.1 Analytical formulation

In the following, we consider a bridge pier embedded at a distance D in the soil and under free vibration in the lateral direction x (Figure 6). So the model takes into account only the rigid body motion of the pier.

The following assumptions are made in the theoretical formulation:

- The pier is a rigid beam with a total mass m, a moment of inertia around the gravity center J_G and L_1 the distance between the base and the gravity center.
- The soil is assumed to be homogeneous and its weight is neglected.
- The lateral soil reaction is modelled as horizontal independent linear elastic springs according to the Winkler theory [14] with a stiffness k_s.
- The base rotational springs K_r take into account the moment produced by normal pressure on the base of the pier, induced by base rotation.

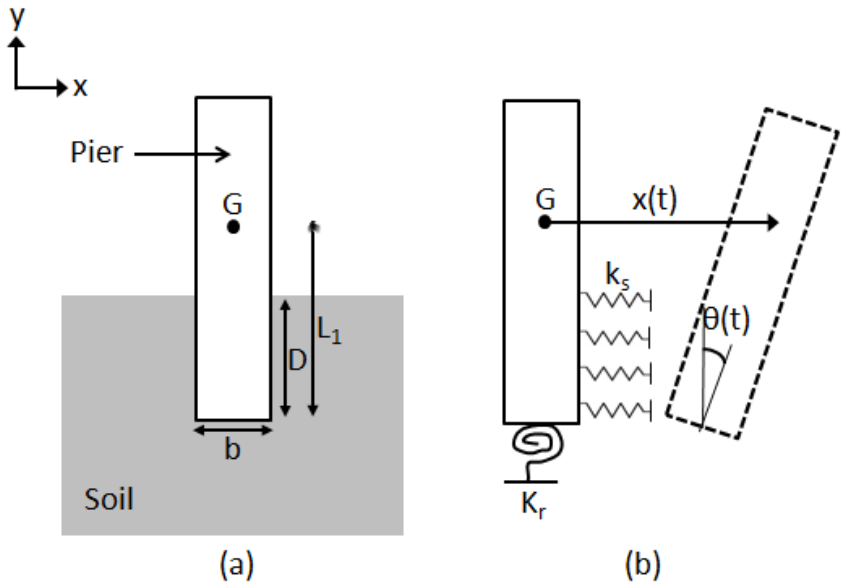

Figure 6: Rigid body vibration of a pier in soil : (a) Definition sketch (b), Proposed equivalent analytical model.

In the plane, the pier has two degrees of freedom: the displacement $x(t)$ and the rotation $\theta(t)$ of its gravity center.

The equilibrium of horizontal forces can be written:

$$m\ddot{x} + \int_{-L_1}^{-L_1+D} k_s(x + \theta y)\ \mathrm{d}y = 0. \tag{1}$$

The rotation equilibrium around the gravity center can be expressed as:

$$J_G\ddot{\theta} + K_r\theta + \int_{-L_1}^{-L_1+D} k_s(x + \theta y)y\ \mathrm{d}y = 0. \tag{2}$$

Equations (1) and (2) lead to the following system:

$$\begin{cases} m\ddot{x} + k_s D x + \frac{k_s\theta}{2} D(D - 2L_1) = 0, \\ J_G\ddot{\theta} + K_r\theta + \frac{k_s x}{2} D(D - 2L_1) + \frac{k_s\theta}{3}[(D - L_1)^3 + {L_1}^3] = 0, \end{cases} \tag{3}$$

which can be written as:

$$\begin{bmatrix} m & 0 \\ 0 & J_G \end{bmatrix} \begin{Bmatrix} \ddot{x} \\ \ddot{\theta} \end{Bmatrix} + \begin{bmatrix} k_s D & \frac{k_s}{2} D(D - 2L_1) \\ \frac{k_s}{2} D(D - 2L_1) & K_r + \frac{k_s}{3}[(D - L_1)^3 + {L_1}^3] \end{bmatrix} \begin{Bmatrix} x \\ \theta \end{Bmatrix} = 00 \tag{4}$$

The solution of Equation (4) can be expressed as:

$$\begin{cases} x(t) = X\cos(\omega t + \varphi) \\ \theta(t) = \Theta\cos(\omega t + \varphi) \end{cases} \tag{5}$$

The following system is then obtained by substituting equation (5) in equation (4):

$$\begin{bmatrix} k_s D - m\omega^2 & \frac{k_s}{2} D(D - 2L_1) \\ \frac{k_s}{2} D(D - 2L_1) & -J_G\omega^2 + K_r + \frac{k_s}{3}[(D - L_1)^3 + {L_1}^3] \end{bmatrix} \begin{Bmatrix} X \\ \Theta \end{Bmatrix} = 0. \tag{6}$$

Equation (6) has a non-trivial solution only if:

$$mJ_G\omega^4 - \left(k_s D J_G + K_r m + \frac{k_s m}{3}[(D-L_1)^3 + {L_1}^3]\right)\omega^2 + (k_s K_r D + \frac{k_s^2}{3} D[(D-L_1)^3 + {L_1}^3]) - \left(\frac{k_s}{2} D(D-2L_1)\right)^2 = 0. \quad (7)$$

The eigenfrequencies f_1 and f_2 of the two rigid modes of the pier are the solutions of Equation (7).

The modal shapes $(X_i, \Theta_i)_{i\subset\{1,2\}}$ corresponding to the two eigenfrequencies of the beam are calculated using the following equation:

$$(k_s D - m{\omega_i}^2)X_i + \frac{k_s}{2} D(D-2L_1)\Theta_i = 0 \quad (8)$$

Hereafter, we choose to normalize the modal shapes to the maximal displacement.

4.2 Theoretical relation between k_s and K_r

In order to perform a sensitivity study, a first attempt is made to establish a simple relation between the horizontal stiffness of the soil k_s and the rotational stiffness K_r, an energetic approach is used. We make the assumption that the base of the pier is resting on uniformly distributed closely spaced springs having the same stiffness k_s as the horizontal ones as shown in figure 7.

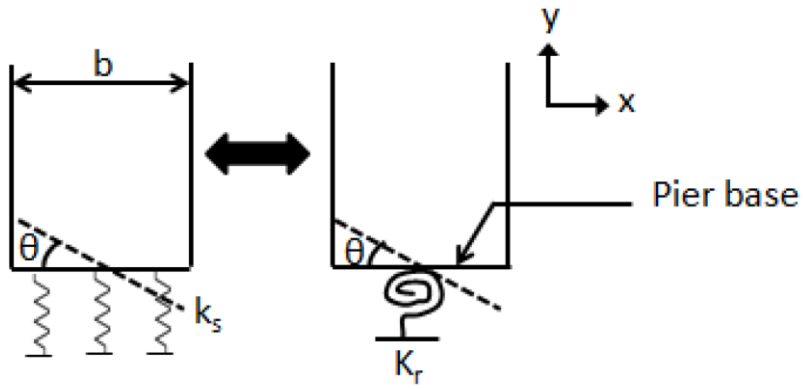

Figure 7: Rotational spring K_r equivalence to vertical spring k_s.

The elastic energy of deformation at the base of the pier can be written:

$$\frac{1}{2}\int_{-\frac{b}{2}}^{+\frac{b}{2}} k_s(\theta y)^2 \, dx = \frac{1}{2} K_r \theta^2. \quad (9)$$

Therefore, the initial estimated rotational stiffness $(K_r)_{init}$ is proportional to k_s according to the following equation:

$$(K_r)_{init} = \frac{1}{12} k_s b^3. \quad (10)$$

4.3 Numerical validation of the theoretical model

In order to validate the theoretical formulation of the model and perform a sensitivity analysis to the soil stiffness and the slenderness ratio of the pier, a 2D-finite element model is developed. The pier is modeled as an Euler Bernoulli beam and the soil-structure interaction is modelled with linear elastic springs of a stiffness K that verifies:

$$K = k_s \times \Delta y, \tag{11}$$

where k_s is the modulus of subgrade reaction of the soil and Δy is the spacing between the springs. A rotational spring is modeled at the base of the beam. The finite element model is then computed for different soil stiffness. The results of the parametric study are summarized in table 4.

This numerical model show good agreement with analytical model, for various value of the soil stiffness k_s (Table 2).

Lateral stiffness k_s	First frequency (Hz)		Second frequency (Hz)	
MN.m $^{-2}$	Analytical	Numerical	Analytical	Numerical
1	7.21	7.19	29.95	30.00
5	16.12	16.11	66.99	67.01
10	22.80	22.78	94.96	94.87
100	72.13	71.01	300.29	299.38
500	161.29	144.56	671.47	662.02

Table 2: Comparison of analytical and numerical frequencies for different values of soil stiffness.

The results also indicate that as soil stiffness increases, the gap between analytical and numerical results increases : This is because, as soil stiffness increases, the assumption that the pier behaves as a rigid body with respect to the soil stiffness is no longer valid. In this case, the pier behaves as an elastic beam.

A second sensitivity study was performed to evaluate the effect of the slenderness ratio α on the validity of the proposed model (Table 3) : the numerical and analytical models are in agreement for low slenderness ratios α.

Slenderness ratio α	First frequency (Hz)		Second frequency (Hz)	
-	Analytical	Numerical	Analytical	Numerical
2	38.57	38.88	101.16	100.3
5	26.83	26.80	96.28	96.17
10	25.85	25.22	96.01	95.71
50	25.71	5.35 (bending mode)	95.97	32.29 (bending mode)

Table 3: Comparison of analytical and numerical frequencies for different slenderness ratio α for an embedded length of D=L/2 and $k_s = 10$ MN/m ^{2}..

However, for a slenderness ratio $\alpha = 50$, the vibration of the pier is governed only by elastic modes. Therefore, the analytical model is no longer valid for this kind of structures.

4.4 The effect of the rotational spring

A sensitivity study is performed to assess the contribution of the rotational spring to the soil stiffness. The horizontal stiffness is $k_s = 50$ MN/m ^{2} and the stiffness of the rotational spring $(K_r)_{init}$ is calculated using Equation (10). The frequencies of the pier are computed, with and without the rotational spring, for an embedded length D from 5 to 25 cm.

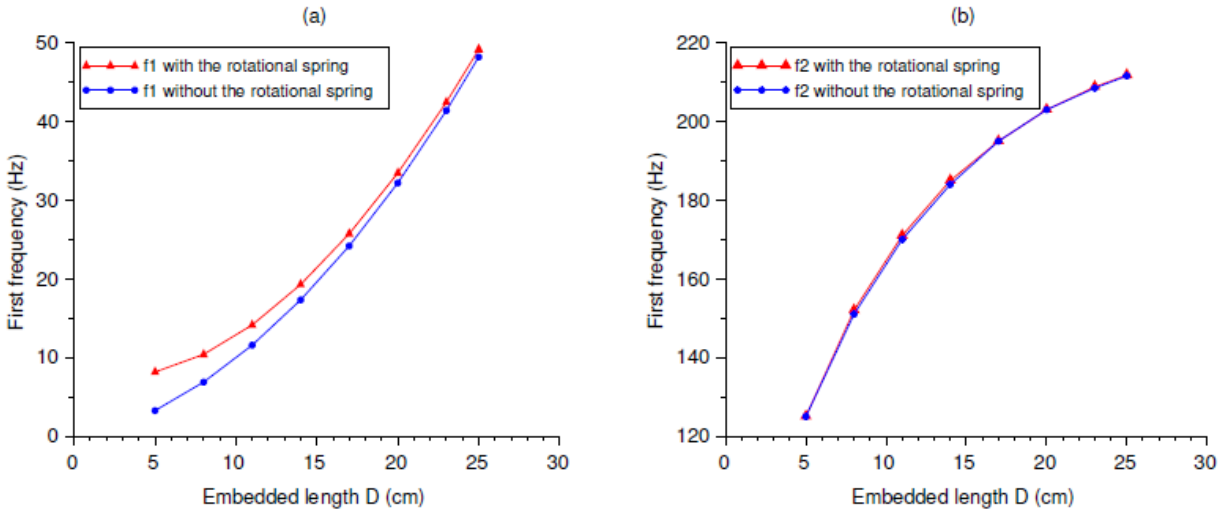

Figure 8: Effect of the rotational spring with varying embedded length (a) on the first frequency f_1 and (b) the second frequency f_2 of the pier.

Only the first rigid frequency f_1 is significantly modified by the rotational spring (Figure 8). This effect is more predominant as the embedded length D decreases. This is mainly linked to the fact that the less the pier is embedded, the less the lateral soil is mobilized in comparison with the soil base. When the pier is embedded enough, the vibration of the pier in governed mainly by the lateral soil interaction and the effect of soil base is therefore negligible.

5 Proposed model validation

5.1 Identification of the soil stiffness parameters

A 3D-finite element model is developed using Code-Aster software. Both the soil and the model bridge pier are modeled using 3D elements and are meshed using 10 nodes tetrahedron elements. The model is based on the following hypothesis: 1) the soil medium and the pier are elastic, 2) the soil's Young modulus E_s remains constant with depth and 3) the soil and the pier are perfectly bounded at the interface. The soil reaches 2 m depth and 2.5 m width, therefore preventing any border effect on the pier response. The displacement of the lateral faces of the soil are blocked in the normal direction and the base is blocked in all directions. Scour is simulated by creating a cylindrical hole around the pier as shown in Figure 9(a).

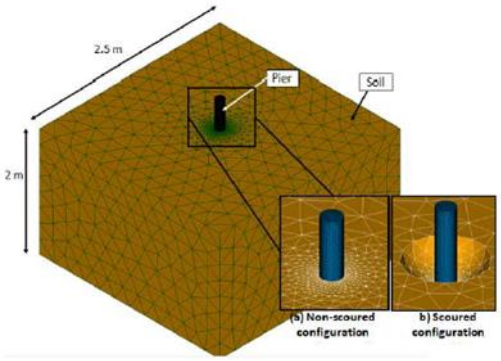

(a) Mesh details

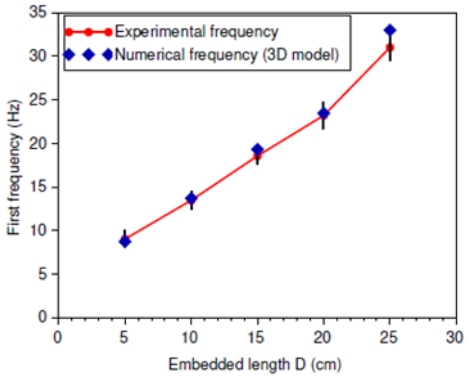

(b) Comparison of experimental and numerical results

Figure 9:Finite elements model if the soil-pier system (a) mesh details and (b) results of the single pier in dry sand.

The material and geometrical parameters of the pier used are the experimental ones. The mass density and the Poisson ratio of the soil are $\rho_s = 1700$ Kg/m ^{3} and $\nu_s = 0.33$ respectively. Since the Young modulus E_s of the soil is the only unknown parameter, its value is calibrated in order to have the best fitting numerical results for the experimental single pier results. A good agreement is obtained for $E_s = 4.2$ MPa. A modal analysis is performed for each 5 cm scour depth to evaluate the frequency of the pier (Figure 8(b)).

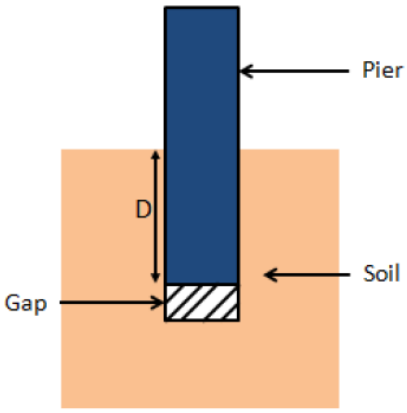

Figure 10: Figure of the second numerical model neglecting the base effect.

Once the 3D model is calibrated, the numerical values of k_s and K_r can be determined following two steps : First, for k_s, a second 3D-model, with a gap between the pier's base and the soil, is developed (Figure 10). This makes it possible to eliminate the contribution of the base stiffness to the pier response, therefore this model is equivalent to the analytical model with $K_r = 0$.

This numerical model is computed for high embedded lengths $D = 25$cm and $D = 20$cm to avoid any base effect.

Considering the analytical model, the numerical frequency $(f_1)_{num}$ is solution of Equation (7), and thus verifies:

$$mJ_G{\omega_{num}}^4 - \left(k_s D J_G + \frac{k_s m}{3}[(D-L_1)^3 + {L_1}^3]\right){\omega_{num}}^2 + \left(\frac{k_s^2}{3}D[(D-L_1)^3 + {L_1}^3]\right) - \left(\frac{k_s}{2}D(D-2L_1)\right)^2 = 0, \quad (12)$$

where $\omega_{num} = 2\pi(f_1)_{num}$.

The value of k_s can then be derived by solving Equation (12), see Table 3. This analysis determines a range of possible numerical values for k_s, and allowing use to choose $k_s =$ 25~MPa in the following.

D (cm)	f without a gap (Hz)	f with a gap (Hz)	k_s (MPa)
25	33.0	30.00	20
20	23.5	22.5	25

Table 4: Numerical values for pier frequencies, with and without the base effect.

In a second step, the value of K_r is determined. Since the effect of K_r is predominant for low embedded length, Equation (7) is solved for small values of D ($D = 5$cm and $D = 10$ cm). The input parameters are $k_s = 25$ MPa (as determined previously) and $\omega = 2\pi f_{num} (D = 5cm; D = 10cm)$ where f_{num} the numerical frequency computed with the first 3D-model (Figure 8). The average value of the rotational spring obtained is $K_r \simeq 4100$ N.m/rad. It is worthy to mention that this value correspond to 3 times the value of the initial stiffness $(K_r)_{init}$, as obtained with Equation (10). The values of k_s and K_r are kept fixed in the following.

5.2 Comparison with the experimental results of the single pier

In order to assess the accuracy of the proposed model, the experimental data is compared to the theoretical results. The theoretical frequencies are computed for the previously calibrated value of k_s ($k_s = 25$ MPa) and two values of the rotational spring: $(K_r)_{init}$ computed using Equation (10) and the calibrated value of $(K_r)_{calib}$ so that the relation between the two rotational spring stiffness was find to verify:

$$(K_r)_{calib} = 3 \times (K_r)_{init} = \frac{1}{8}k_s b^3. \quad (13)$$

Figure 11(a) indicates that the model computed with the initial value of the rotational spring $(K_r)_{init}$ does not simulate correctly the single pier behaviour. In fact, as the embedded length D of the pier decreases the gap between the theoretical and experimental frequencies increases, which is predominately related to an underestimation of the base rotational spring, as demonstrated in Section 4.4. This assumption is confirmed when the model is computed with a higher value of rotational spring stiffness $(K_r)_{calib}$. The results show a good agreement between experimental results and the calibrated theoretical model. For the single pier in flume, the model does not take into account the loose stiffness of the first 5 cm of the soil and therefore overestimates these frequencies.

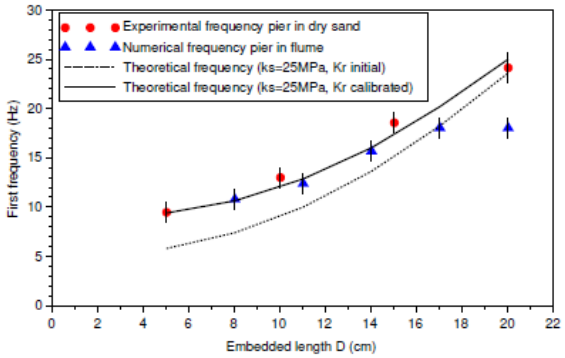

(a) Comparison between experimental and theoretical first frequency

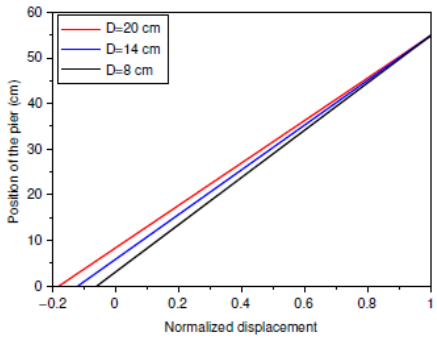

(b) Theoretical first modal shape

Figure 11: Single bridge pier (a) theoretical frequency and (b) corresponding modal shape.

The theoretical modal shape of the pier is also calculated. The results (Figure 11(b)) confirm that the first analytical modal shape correspond to a coupled swaying-rocking motion and validates the model calibration.

5.3 Comparison with the experimental results of the pier in bridge configuration

For the validation of the modelling of the pier in bridge configuration, we assume that each pier supports half the deck weight. The deck is modeled as a nodal mass placed at the top of the pier and having a total weight $M' = M/2$ with M the total mass of the deck (Figure 12(a)). In this case, the values of the weight m and the moment of inertia around the gravity center of the pier J_G are modified to take into account the bridge deck. In that respect, the modified values are expressed by:

$$\begin{cases} m' = m + M', \\ J'_G = J_G + M' \times d, \end{cases} \tag{14}$$

where m' and J_G, are the modified weight and moment of inertia around the gravity center respectively and d the distance between the gravity center of the pier and the gravity center of half the deck. A good agreement (Figure 12(b)) between the theoretical and experimental results is achieved. Therefore, the model is capable of predicting the pier frequency variation with scour when the bridge deck is correctly taken into account.

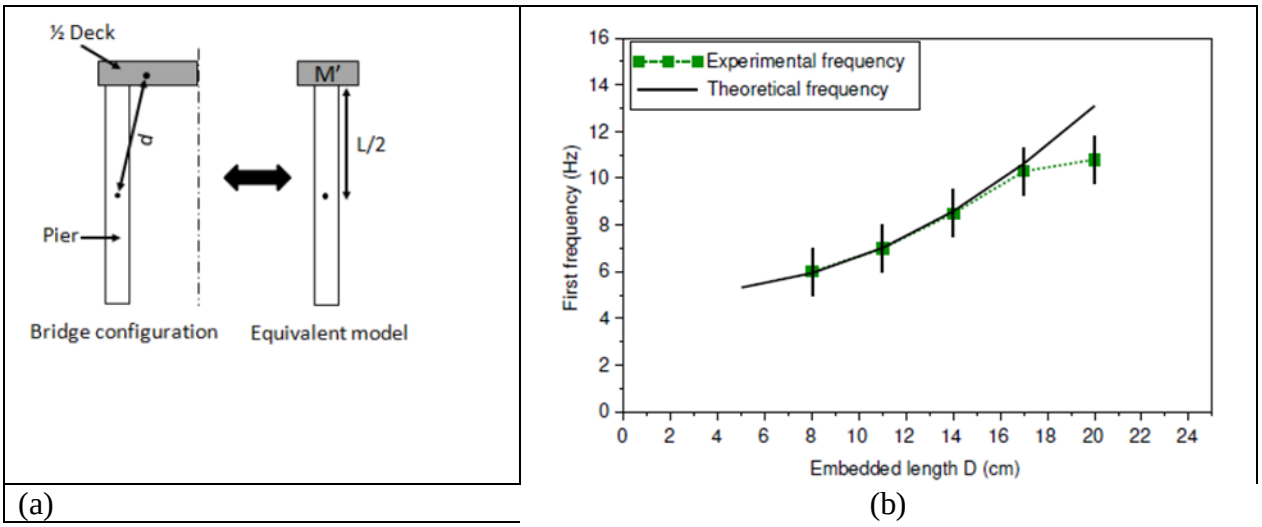

(a) (b)

Figure 12: Pier in bridge configuration (a) Simplified model and (b) comparison between experimental and theoretical first frequency.

5.4 Confrontation to literature results

In this section, the analytical model is used to model the tests conducted by [3]. The tested single bridge pier had a diameter of $b = 15.3$ cm and a total length $L = 30.6$ cm. The embedded length was varied from $D = 22$cm to $D = 7$cm with 3 cm scour increment. The pier was tested in a low density sand.

The proposed theoretical model is computed using a lateral spring stiffness $k_s = 8.5$ MPa and the rotationnel spring K_r is calculated using the equation deduced after spring calibration expressed (Equation (13)).

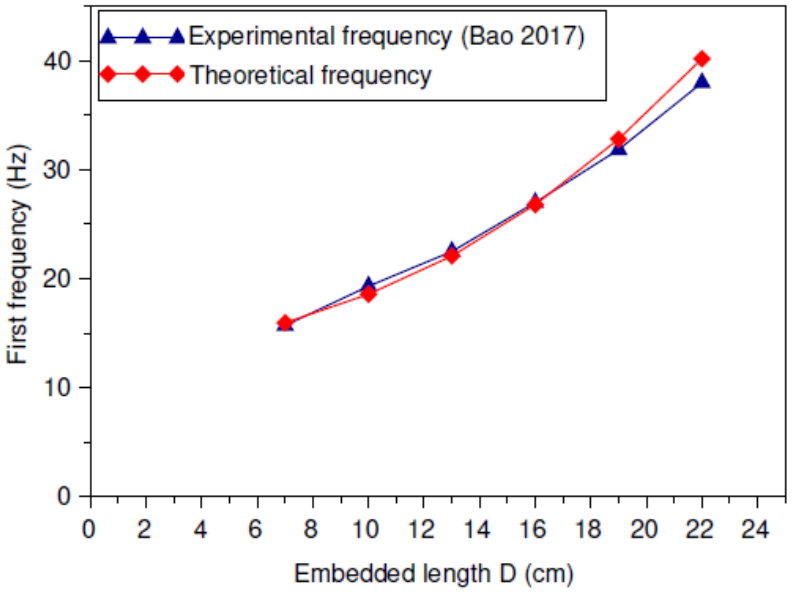

Figure 13: Comparison between theoretical and experimental frequencies of [3].

The results of the proposed model after calibration are in a good agreement with the experimental results (Figure 13).

6 Final remarks and conclusions

This paper investigates the effects of scour on the frequency of a bridge pier and proposes a simplified model for this kind of structures.

To this end, experimental campaigns were conducted in a water flume using a single pier in two types of soil, dry sand and saturated sand. The pier was also tested in a bridge configuration to evaluate the deck effect on the pier frequency. These experimental results provided validation data for both the first frequency and the corresponding modal shape of the pier.

A theoretical model was proposed to model the pier behaviour. The soil-structure interaction was modelled by both horizontal springs along the pier and a rotational spring at the base to take into account the vertical effect of the soil that become predominant as scour increases. This model has been proven to be in good agreement with the experimental results, for both the frequencies and the modal shape of the single piers and the piers in bridge configuration.

It has therefore been shown that the first rigid frequency of the pier corresponds to a coupled swaying-rocking mode. The bridge configuration has been modelled correctly by applying nodal masses at the top of the piers, equal to half the mass of the deck .

The proposed theoretical model has also been compared to literature results, good agreement has been shown.

The main limitation of the model is the direct identification of the lateral stiffness of the soil instead of fitting the experimental results. Future research will try establishing empirical relations between the lateral spring stiffness and the Young modulus of the soil for rigid piers.

References

1] Neil L. Anderson, Ahmed M. Ismael, and Thanop Thitimakorn. Ground-penetrating radar: A tool for monitoring bridge scour. *Environmental and Engineering Geoscience*, 13:1–10, 2007.

[2] Faezeh Azhari and Kenneth J Loh. Laboratory validation of buried piezoelectric scour sensing rods. *Structural Control and Health Monitoring*, 24(9), 2017.

[3] Ting Bao and Zhen Liu. Vibration-based bridge scour detection: A review. *Structural Control and Health Monitoring*, 24(7), 2017.

[4] Ting Bao, R. Andrew Swartz, Stanley Vitton, Ye Sun, Chao Zhang, and Zhen Liu. Critical insights for advanced bridge scour detection using the natural frequency. *Journal of Sound and Vibration*, 386:p.p:116 – 133, 2017.

[5] Nissrine Boujia, Franziska Schmidt, Christophe Chevalier, Dominique Siegert, and Damien Pham van Bang. Distributed Optical Fiber-Based Approach for Soil-Structure Interaction. *Sensors*, 20(321), 2020.

[6] Nissrine Boujia, Franziska Schmidt, Christophe Chevalier, Dominique Siegert, and Damien Pham van Bang. Effect of Scour on the Natural Frequency Responses of Bridge Piers: Development of a Scour Depth Sensor. *Infrastructures*, 4(21), 2019.

[7] Genda Chen, Brandon P. Schafer, Zhibin Lin, Ying Huang, Oscar Suaznabar, Jerry Shen, and Kornel Kerenyi. Maximum scour depth based on magnetic field change in smart rocks for foundation stability evaluation of bridges. *Structural Health Monitoring*, 14(1):86–99, 2015.

[8] Lu Deng and C.S. Cai. Bridge scour: Prediction, modeling, monitoring, and countermeasures - review. *Practice Periodical on Structural Design and Construction*, 15(2):125–134, 2010.

[9] Emma Florens, Christophe Chevalier, Frédérique Larrarte, Franziska Schmidt, and

Edouard Durand. Scour monitoring on bridge pier - methodology and implementations. In *Scour and Erosion: Proceedings of the 9th International Conference on Scour and Erosion, Taipei, Taiwan, 5-8 Novembre 2018*. CRC Press, 2018.

[10] Sebastiano Foti and Donato Sabia. Influence of Foundation Scour on the Dynamic Response of an Existing Bridge. *Journal of Bridge Engineering*, 16(2):295–304, 2011.

[11] S.R. Gorin and F.P. Haeni. Use of surface-geophysical methods to assess riverbed scour at bridge piers. Technical report, US Geological Survey; Books and Open-File Reports, Federal Center, 1989.

[12] Jau-Yau Lu, Jian-Hao Hong, Chih-Chiang Su, Chuan-Yi Wang, and Jihn-Sung Lai. Field measurements and simulation of bridge scour depth variations during floods. *Journal of Hydraulic Engineering*, 134(6):810–821, 2008.

[13] S.G. Millard, J.H. Bungey, C. Thomas, M.N. Soutsos, M.R. Shaw, and A. Patterson. Assessing bridge pier scour by radar. *NDT & E International*, 31(4):251–258, 1998.

[14] Luke J. Prendergast, David Hester, and Kenneth Gavin. Determining the Presence of Scour around Bridge Foundations Using Vehicle-Induced Vibrations. *Journal of Bridge Engineering*, 21(10), 2016.

[15] Luke J. Prendergast, D. Hester, Kenneth Gavin, and John James O'Sullivan. An investigation of the changes in the natural frequency of a pile affected by scour. *Journal of Sound and Vibration*, 332(25):6685 – 6702, 2013.

[16] Masahiro Shinoda, Hiroshi Haya, and Seiji Murata. Nondestructive evaluation of railway bridge substructures by percussion test. In *Proceedings of the Fourth International Conference on Scour and Erosion, Tokyo, Japan*, 2008.

[17] Michael Taricska. *An Analysis of Recent Bridge Failures (2000-2012)*. PhD thesis, The Ohio State University, 2014.

[18] Kumalasari Wardhana and Fabian C Hadipriono. Analysis of recent bridge failures in the United States. *Journal of Performance of Constructed Facilities*, 17(3):144–150, 2003.

[19] E Winkler. Theory of elasticity and strength. *Dominicus Prague*, 1867.

[20] Ali Zarafshan, Amirhossein Iranmanesh, and Farhad Ansari. Vibration-based method and sensor for monitoring of bridge scour. *Journal of Bridge Engineering*, 17(6):829–838, 2012.